

Article

Nonisothermal Cure Kinetics of Epoxy/Polyvinylpyrrolidone Functionalized Superparamagnetic Nano-Fe₃O₄ Composites: Effect of Zn and Mn Doping

Maryam Jouyandeh ¹, Mohammad Reza Ganjali ^{1,2}, Farzad Seidi ³, Huining Xiao ⁴ and Mohammad Reza Saeb ^{5,*}

¹ Center of Excellence in Electrochemistry, School of Chemistry, College of Science, University of Tehran, Tehran 11155-4563, Iran; maryam.jouyande@gmail.com (M.J.); ganjali@ut.ac.ir (M.R.G.)

² Biosensor Research Center, Endocrinology and Metabolism Molecular-Cellular Sciences Institute, Tehran University of Medical Sciences, Tehran 11155-4563, Iran

³ Provincial Key Lab of Pulp and Paper Science and Technology and Joint International Research Lab of Lignocellulosic Functional Materials, Nanjing Forestry University, Nanjing 210037, China; f_seidi@njfu.edu.cn

⁴ Department of Chemical Engineering, University of New Brunswick, Fredericton, NB E3B 5A3, Canada; hxiao@unb.ca

⁵ Department of Resin and Additives, Institute for Color Science and Technology, Tehran P.O. Box: 16765-654, Iran

* Correspondence: saeb-mr@icrc.ac.ir; Tel.: +98-(21)-2295-6209; Fax: +98-(21)-2294-7537

Received: 26 April 2020; Accepted: 11 May 2020; Published: 18 May 2020



Abstract: The effects of the bulk and surface modification of nanoparticles on the cure kinetics of low-filled epoxy nanocomposites containing electrochemically synthesized polyvinylpyrrolidone (PVP) functionalized superparamagnetic iron oxide (PVP-SPIO), Zn-doped PVP-SPIO (Zn-PVP-SPIO), and Mn-doped PVP-SPIO (Mn-PVP-SPIO) were studied using differential scanning calorimetry (DSC) and cure kinetics analyses. Integral and differential isoconversional methods were used to calculate the activation energies (E_a) and consequently propose the appropriate reaction model for the curing reaction under nonisothermal conditions. According to the alteration of E_a versus the fractional extent of conversion, the E_a trend was changed through the partial replacement of Fe²⁺ sites by the Zn²⁺ and Mn²⁺ cations in the general formula of M_xFe_{3-x}O₄, due to smaller amounts of energy being required for curing by the incorporation of Zn-PVP-SPIO and Mn-PVP-SPIO nanoparticles into the epoxy resin. A good agreement was observed between the theoretical calculation and the observed calorimetric data for the model validation.

Keywords: cure kinetics; epoxy; isoconversional model, superparamagnetic iron oxide; bulk modification, surface modification

1. Introduction

The study of the cure reaction of resin composites is key to perceiving the relation between the crosslinking reaction and the ultimate properties of composite materials [1–3]. The mysterious nature of the interaction between polymer chains and particles in the thermoset resins makes investigations on cure reactions challenging [4–6]. *Cure Index (CI)* is a new dimensionless criterion that can simply identify the state of cure of thermoset resins in the presence of fillers from a qualitative analysis point of view [7]. Typically, *Poor*, *Good*, and *Excellent* cure are three labels assigned to the thermoset composites in terms of the value of the *CI* [8,9]. Moreover, the investigation of the kinetics of the curing reaction

can be quantitatively analyzed to complete the detailed investigation of the network formation in the thermoset composites [10,11].

The cure behavior and kinetics of epoxy-based nanocomposites containing different types of nanoparticles were investigated in a series of studies. The main consideration of these studies was the investigation of cure reaction in the presence and the absence of surface modifiers and additives with different functional groups in epoxy composites. The effects of the bulk and surface modification of nanoparticles on the cure reaction of the epoxy/amine system were investigated qualitatively with the aid of the *CI*. The potential of different layered double hydroxides (LDH), such as Mg-Al-LDH [12,13], Zn-Al-LDH [14,15], Mg-Zn-Al-LDH [16], and Ni-Al-LDH [17], with NO_3 and CO_3 intercalating anions on the curability of the epoxy/amine system was investigated, which led to understanding that anions in the structure of LDH are more efficient than the cations in the epoxide ring opening. Analyses on epoxy nanocomposites containing Fe_3O_4 and Mn^{2+} -doped Fe_3O_4 demonstrated that Mn^{2+} cations played the role of catalyst in the curing reaction of epoxy/amine, which led to a shift from *Poor* to *Good* and *Excellent* [18]. Nonisothermal differential scanning calorimetry (DSC) demonstrated that the addition of Ni-doped Fe_3O_4 hindered the epoxy curing reaction with amine. The Ni^{2+} dopants tended to be located in the top layer of Fe_3O_4 and increased their tendency to aggregate, which caused a *Poor* cure state [19]. The Co^{2+} -doped Fe_3O_4 significantly increased the amount of heat released by the epoxy system during the curing reaction compared to the epoxy/ Fe_3O_4 system [20]. It was found that the incorporation of Fe_3O_4 into the epoxy decreased the curing enthalpy of epoxy, while Gd^{3+} -doped Fe_3O_4 facilitated the curing reaction between the epoxy and amine curing agent due to improved dispersion in the epoxy matrix [21]. Moreover, it was found that by substituting Zn^{2+} dopants with Fe^{2+} in the Fe_3O_4 lattice, the curability of the epoxy/amine systems was changed from a *Poor* to *Good* state [22]. It was also shown that the surface modification of magnetic nanoparticles with functional organic groups, such as polyvinyl chloride [23], polyethylene glycol [24–26], and ethylenediaminetetraacetic acid [27], enhanced the cure reaction of the epoxy resin due to the better dispersibility of nanoparticles and participation of reactive groups on the surface of the functionalized nanoparticles in the epoxide ring opening. The effects of the simultaneous surface modification of the Fe_3O_4 nanoparticles with polyvinylpyrrolidone (PVP) and the bulk modification with Mn [28], Ni [29], and Zn [30] dopants on the cure reaction of epoxy with an amine curing agent were also studied through the lens of *CI*. A *Good* cure was the case for epoxy containing 0.1 wt.% Mn-doped PVP- Fe_3O_4 , due to the accelerating effect of PVP and Mn^{2+} simultaneously on the crosslinking reaction of epoxy [28]. A shift in the cure state of the epoxy nanocomposites from *Poor* to *Good* was also observed by replacing PVP- Fe_3O_4 with PVP-Ni- Fe_3O_4 in the system; this was indicative of the complementary role of superparamagnetic iron oxide nanoparticles' (SPION') doping in Ni.

In the present study, the effect of PVP-functionalized superparamagnetic iron oxide with different dopants of Mn and Zn on the cure kinetics of the epoxy/amine system was examined and compared with the neat epoxy as a reference sample [31,32]. Isoconversional model free methods were applied to the nonisothermal scanning calorimetry data for obtaining the kinetics parameters, including the activation energy and order of reaction rate.

2. Experimental Section

See Appendix A for materials and methods. Nonisothermal DSC was used in our study for the qualitative analysis of the curing reactions of the epoxy/amine system and its nanocomposites containing polyvinylpyrrolidone functionalized superparamagnetic iron oxide (PVP-SPIO), Zn-doped PVP-SPIO (Zn-PVP-SPIO), and Mn-doped PVP-SPIO (Mn-PVP-SPIO) nanoparticles. Details about the materials and their physical properties are proposed in Section Appendix A.1 of Appendix A. Section Appendix A.2 of Appendix A describes the preparation of epoxy nanocomposites containing PVP-SPIO, Zn-PVP-SPIO, and Mn-PVP-SPIO. Briefly, 0.1 wt.% of each nanofiller was employed in the nanocomposite preparation, and nonisothermal DSC at the heating rates (β) of 5, 10, 15, and 20 °C/min was used for the curing reaction analysis. The cure behavior and cure kinetics are represented by the

quantitative cure analysis; this was performed based on the protocol suggested for the cure analysis of thermoset composites [33].

3. Results

3.1. Cure Behavior Analysis

Figure 1 shows DSC thermograms of the neat epoxy and its nanocomposites containing 0.1 wt.% of PVP-SPIO, Zn-PVP-SPIO, and Mn-PVP-SPIO at four heating rates of 5, 10, 15, and 20 °C/min. Single-step kinetics reaction was confirmed by the observation of a unimodal peak in the DSC curves [34]. Obviously, for all samples, by increasing the heating rate from 5 to 20 °C/min, the peak temperature of thermograms (T_p) shifted to higher values due to the intensified kinetic energy of the system per molecule at higher temperatures [35].

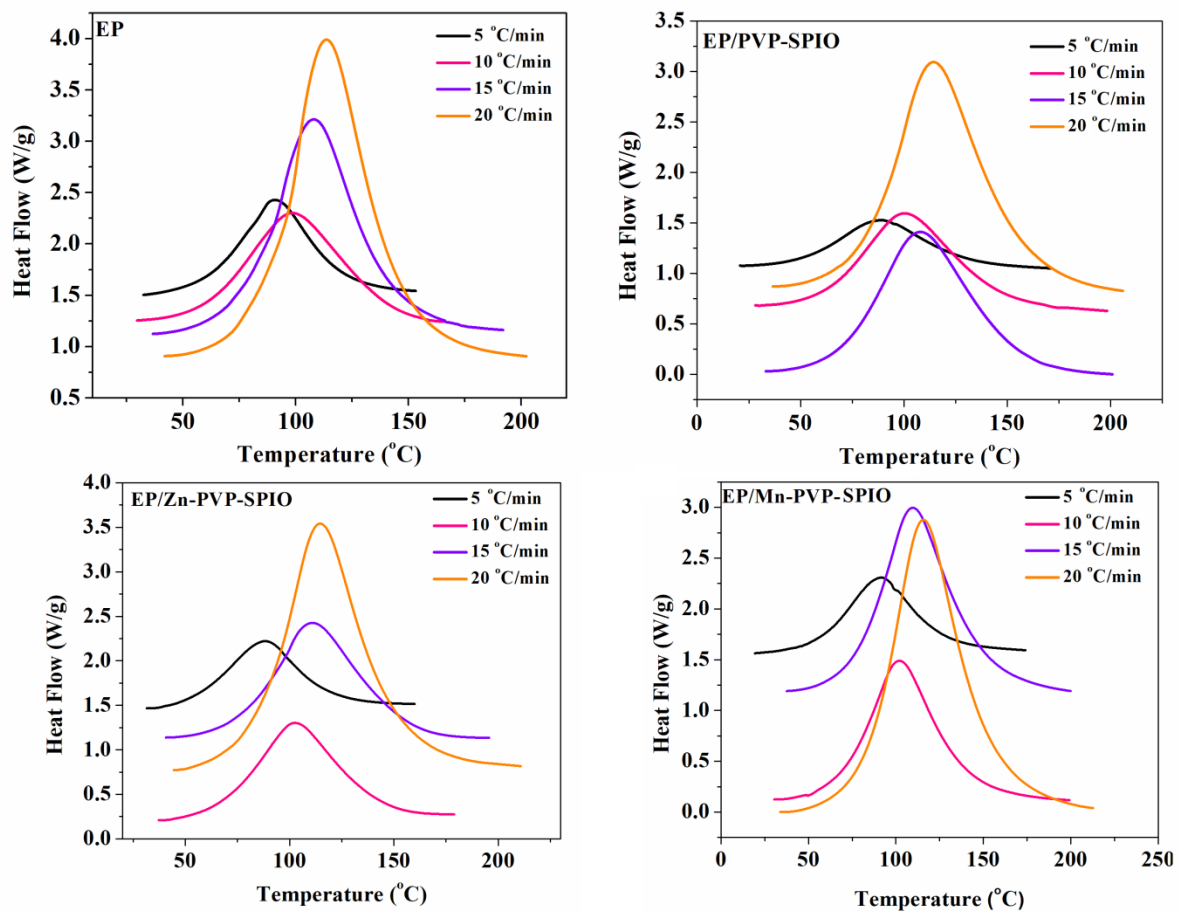


Figure 1. Differential scanning calorimetry (DSC) thermograms for the neat epoxy (EP), EP/polyvinylpyrrolidone (PVP) functionalized superparamagnetic iron oxide (PVP-SPIO), EP/ Zn-doped PVP-SPIO (Zn-PVP-SPIO) and EP/ Mn-doped PVP-SPIO (Mn-PVP-SPIO) nanocomposites at heating rates of 5, 10, 15, and 20 °C/min [28,30].

The enthalpy of the curing reaction and the conversion, α , is assumed to be proportional, and this relevance is calculated by following equation:

$$\alpha = \frac{\Delta H_T}{\Delta H_\infty}, \tag{1}$$

where ΔH_∞ and ΔH_T are defined as the total heat release of the reaction over the whole temperature range and the amount of total heat release of the reaction at a given temperature T , respectively.

Figure 2 shows the variation of α versus temperature at different heating rates for all the studied samples (neat epoxy as reference sample [31,32] and epoxy systems including PVP-SPIO, Zn-PVP-SPIO, and Mn-PVP-SPIO nanoparticles). The sigmoidal shape of conversion charts is indicative of the autocatalytic mechanism of curing reaction [36]. The considerable point is that with the presence of PVP-SPIO and Zn-PVP-SPIO nanoparticles in the epoxy matrix, the conversion profiles kept their shape as a symptom of the dominance of autocatalytic reactions.

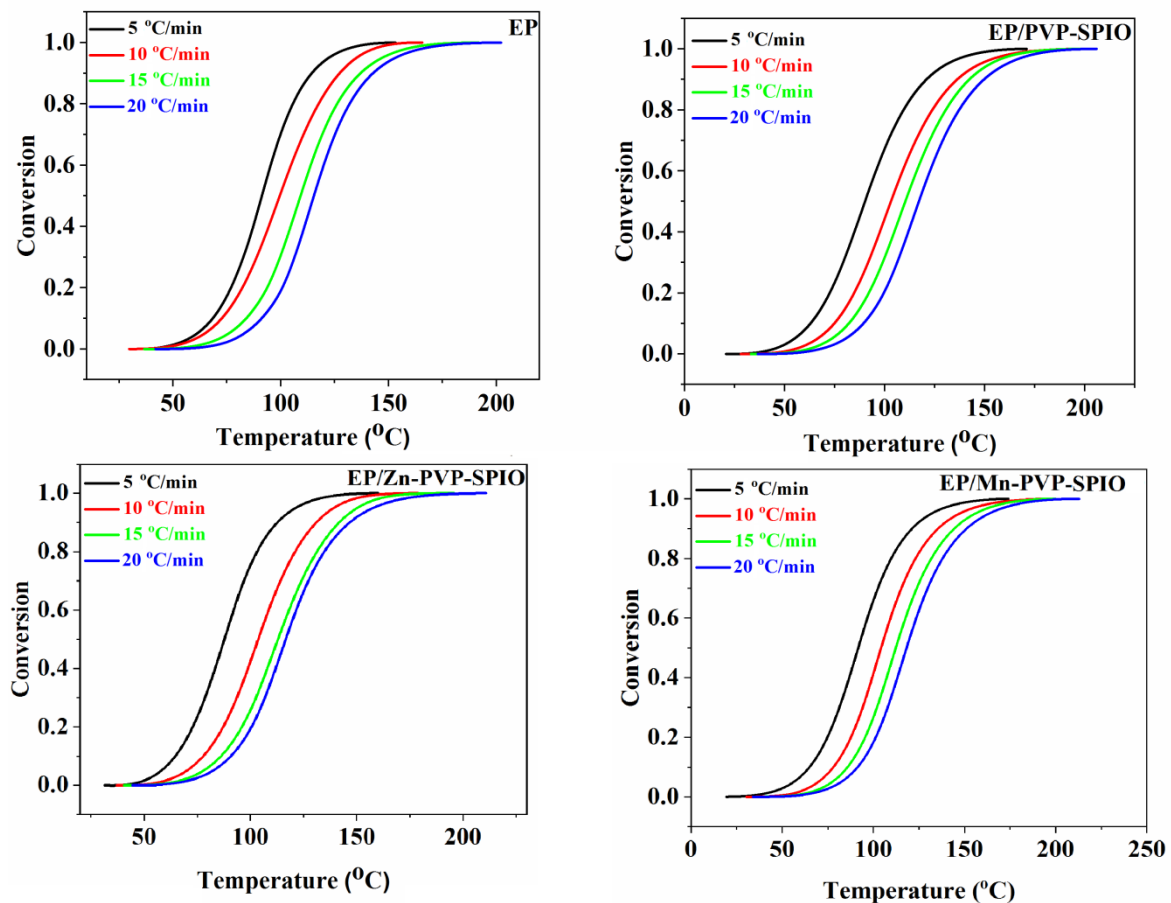


Figure 2. The fractional extent of conversion as a function of reaction time for EP as the reference sample [31,32], as well as EP/PVP-SPIO, EP/Zn-PVP-SPIO, and EP/Mn-PVP-SPIO nanocomposites at heating rates of 5, 10, 15, and 20 °C/min.

3.2. Cure Kinetics Analysis

The primary assumption of isoconversional methods is the dependency of reaction rate on the temperature in a specific α [37–39]. The model-free methods appeared successful in description of variation of activation energy ($E\alpha$) versus α [10]. Kissinger–Akahira–Sunose (*KAS*) integral models and the *Friedman* differential model are two popular isoconversional methods available for the calculation of $E\alpha$ [10]. Using two different views, integral and differential cases enable a deeper explanation of the reaction mechanism. The *Friedman* model is more accurate in comparison with *KAS*. However, there are some other available accurate models, especially for the late stages of the reaction where diffusion plays the key role in the curing phenomenon [40].

As mentioned above, *KAS* and *Friedman* seem to be the most readily available methods for the description of cure reaction. Furthermore, they are trustworthy in the range of $0.1 < \alpha < 0.9$. Details on the calculation of $E\alpha$ derived from both models with mathematical and graphical explanations are available in Appendix B.

Variation patterns of $E\alpha$ versus α based on differential *Friedman* and integral *KAS* models are represented in Figure 3 for EP, EP/PVP-SPIO, EP/Zn-PVP-SPIO, and EP/Mn-PVP-SPIO systems. Figure 3 also indicates that presented data extracted from *Friedman* and *KAS* methods are almost identical. The value of $E\alpha$ is reduced mildly by increasing the degree of conversion, particularly for $\alpha > 0.3$, which is a signature of the autocatalytic nature of the reaction of epoxy with amine curing agent.

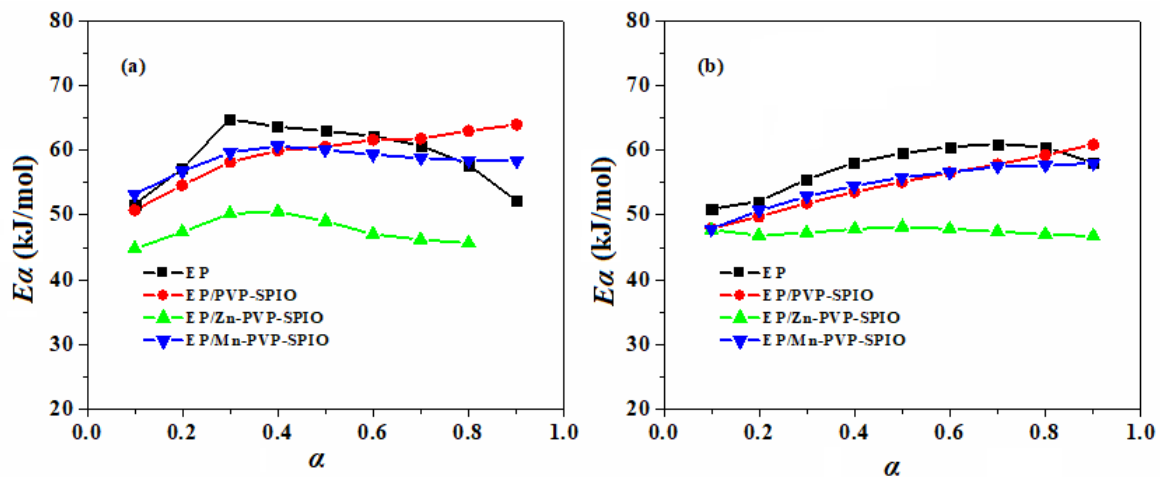


Figure 3. Evolution of activation energy for EP as a reference sample [31,32], as well as EP/PVP-SPIO, EP/Zn-PVP-SPIO, and EP/Mn-PVP-SPIO nanocomposites estimated by (a) the differential *Friedman* model and (b) integral Kissinger–Akahira–Sunose (*KAS*) model.

On the other hand, before the gelation point, crosslinking reactions are progressed through chemical reactions, while after passing the gelation area, a diffusion-controlled mechanism is responsible for the improvement of the reaction [41]. The decrease of activation energy for $\alpha > 0.3$ could be due to the inaccuracy of the used isoconversional models or facilitated autocatalytic ring openings fueled by the hydroxyl functional groups generated in the early stage of reaction, but activated in the middle stage [42].

The average value of the activation energy dropped with the incorporation of PVP-SPIO nanoparticles into the epoxy matrix. This descending order is not only due to the facilitating effect of nanoparticles, but also because of agglomeration arising from nanofillers with detrimental effects on crosslinking. On the other hand, the hindered cure can be traded off through the introduction of Zn and Mn into the bulk structure of Fe_3O_4 . Zn and Mn dopants play an effective role in changing the dispersion state of nanoparticles. The contribution of OH to epoxy ring opening with the Lewis acid effect of Zn^{2+} and Mn^{2+} should be considered in this regard. Therefore, one would assume that the presence of Zn-PVP-SPIO and Mn-PVP-SPIO nanofillers facilitated the cure reaction of epoxy, and hence, $E\alpha$ was decreased [43]. Figure 4 illustrates the structure of Zn-PVP-SPIO and Mn-PVP-SPIO nanofillers and the possible reaction between the cure components and ring-opening reaction. Zn dopant prefers to be placed on the Fe_3O_4 surface, while the third Fe layer changes the efficiency of Fe_3O_4 [22]. By contrast, Mn dopant prefers to be located in the bulk layers of Fe_3O_4 to form Mn^{2+} ions. The effects of dopants on the surface or, in the interior layers of Fe, on the reactivity of Fe_3O_4 toward epoxy should be checked in this context. Since Zn-SPIO and Mn-SPIO nanofillers have different surface reactivity, they may be dispersed in a different manner in the epoxy resin. In our previous works, it was found that vibrational sample magnetometer (VSM) parameters including the saturation magnetization, remanence, and coercivity for Zn-PVP-SPIO are lower than those of Mn-PVP-SPIO [30]. The lower values of VSM parameters indicate single-domain centers for Zn-PVP-SPIO. Hence, it is expected that Zn-PVP-SPIO is dispersed more appropriately than the Mn-PVP-SPIO in the epoxy matrix, resulting in its contribution to the epoxide ring opening, as reflected in lower values of activation energy.

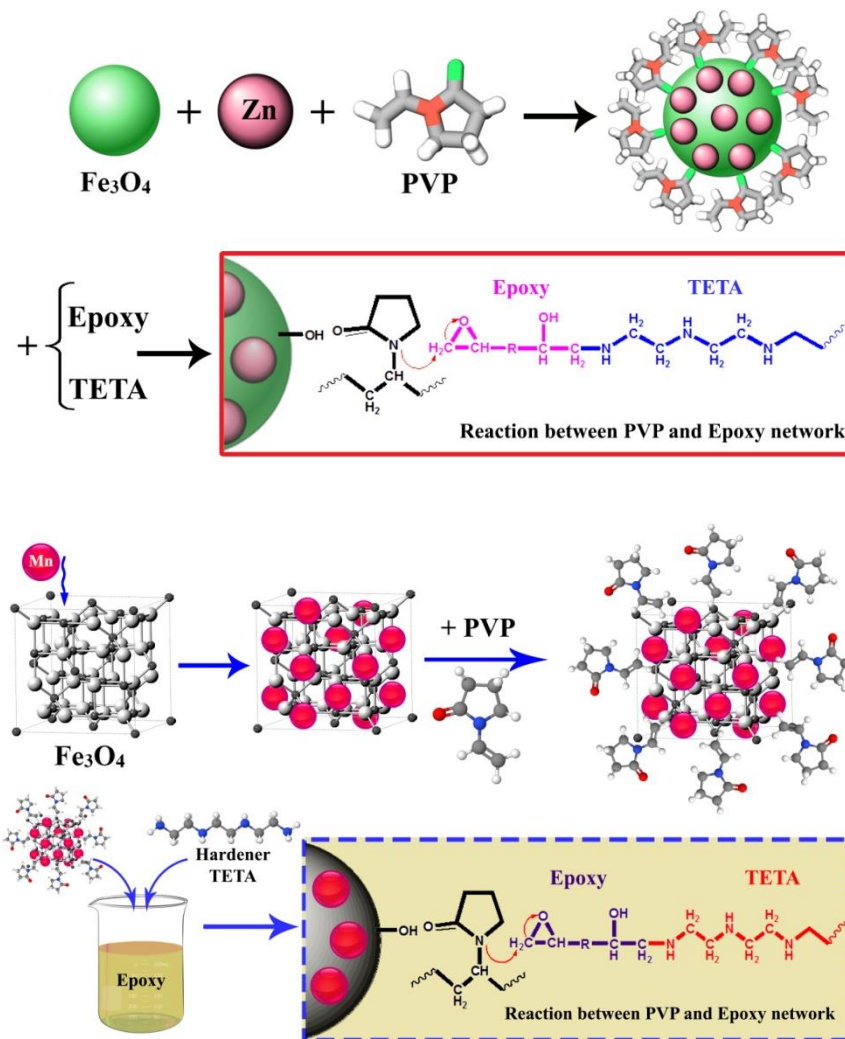


Figure 4. Possible reaction between Zn-PVP-SPIO and epoxy, and also between Mn-PVP-SPIO and curing agent and epoxy resin. It can be observed that the surface (rather than bulk) of nanoparticles is populated by the Zn²⁺ cations. However, bulk layers of Fe₃O₄ are populated by the Mn²⁺ cations.

3.2.1. Determining the Reaction Model and Order of Reaction

The reaction model detection is the prime essential step to study the effect of PVP-SPIO, Zn-PVP-SPIO, and Mn-PVP-SPIO nanoparticles on the curing mechanism of the epoxy/amine system. The *Friedman* and *Malek* methods were chosen to recognize the autocatalytic reaction; the nature of the cure depends on a deep understanding of the details of these methods, as explained in the Appendix C. The curing mechanism can be calculated through Equation (A3), from the shape of the plot of $\ln[Af(\alpha)]$ against $\ln(1 - \alpha)$.

The network formation of neat epoxy and its nanocomposites show autocatalytic behavior, where the maximum points are placed in the range of $0.2 < \alpha < 0.4$, derived from Figure A3.

Furthermore, Appendix C gives information about the calculation of the kinetic model based on the *Malek* method using the maximum points of $y(\alpha) = (\alpha_m)$, $z(\alpha) = (\alpha_p^\infty)$ and the maximum point of conversion in DSC curves (α_p). Further information on the *Malek* method is reported in Appendix C. The values of α_m , α_p and α_p^∞ for epoxy samples at different heating rates are listed in Table 1.

Table 1. The values of α_p , α_m and α_p^∞ obtained from the *Malek* model at various heating rates.

Designation	Heating Rate (°C/min)	α_p^∞	α_m	α_p
EP as reference sample [31,32]	5	0.487	0.144	0.512
	10	0.555	0.073	0.510
	15	0.418	0.236	0.498
	20	0.383	0.251	0.483
EP/PVP-SPIO	5	0.476	0.058	0.499
	10	0.393	0.095	0.483
	15	0.453	0.107	0.491
	20	0.495	0.219	0.475
EP/Zn-PVP-SPIO	5	0.513	0.142	0.530
	10	0.567	0.145	0.500
	15	0.545	0.152	0.492
	20	0.452	0.252	0.481
EP/Mn-PVP-SPIO	5	0.500	0.011	0.514
	10	0.366	0.086	0.480
	15	0.426	0.125	0.473
	20	0.467	0.175	0.475

The two-parameter autocatalytic kinetic model was confirmed via data from Table 1, $\alpha_m < \alpha_p$ and at the same time $\alpha_p^\infty < 0.632$, for EP, EP/PVP-SPIO, EP/Zn-PVP-SPIO, and EP/Zn-PVP-SPIO systems.

As mentioned above, the cure mechanism of the EP, EP/PVP-SPIO, and EP/Zn-PVP-SPIO nanocomposites is autocatalytic according to the *Friedman* and *Malek* models, which is calculated by the below equation:

$$\frac{d\alpha}{dt} = A \exp\left(-\frac{E_\alpha}{RT}\right) \alpha^m (1 - \alpha)^n, \quad (2)$$

where m and n are introduced as the degrees of autocatalytic and noncatalytic reactions, and A is the pre-exponential factor. The values of m , n , and $\ln A$ were determined from Equations (A11) and (A12) in Appendix D. Moreover, the E_α value in this table is the average amount over the whole range of α , based on the *Friedman* and *KAS* methods (Table 2).

By comparing the data in Table 2 for the differential *Friedman* and integral *KAS* methods, it can be speculated that both models show almost the same results. Taking $(m + n)$ as the overall order of crosslinking reaction, the values higher than one for EP, EP/PVP-SPIO, EP/Zn-PVP-SPIO, as well as EP/Mn-PVP-SPIO nanocomposites are evidence of the complexity of the curing reaction [44].

As can be observed in Table 2, the presence of PVP-SPIO nanoparticles in the system changed the mechanism of cure of nanocomposites from autocatalytic to noncatalytic reactions, as clearly evidenced by the reduction in the values of m . By contrast, adding Zn-PVP-SPIO and Zn-PVP-SPIO nanoparticles into the epoxy matrix can revive the autocatalytic reaction, which is verified by a rise in the m value. Moreover, incorporation of PVP-SPIO, Zn-PVP-SPIO, and Mn-PVP-SPIO nanoparticles led to a decline in the collision between curing moieties, evidenced in the decline in $\ln(A)$. The above proves the role of Zn and Mn in facilitating epoxy ring-opening reaction.

Table 2. The kinetic parameters evaluated for the curing of the prepared samples based on the *Friedman* and *KAS* models at different heating rates.

Designation	Heating Rate (°C/min)	$\bar{E}\alpha$ (kJ/mol)	$\ln(A)$ (1/s)	Mean (1/s)	m	Mean	n	Mean
<i>Friedman</i>								
EP as reference sample [31,32]	5	59.23	18.80	18.87	0.410	0.39	1.54	1.596
	10		18.56		0.139		1.44	
	15		18.98		0.445		1.68	
	20		19.12		0.551		1.73	
EP/PVP-SPIO	5	59.36	18.55	18.60	0.151	0.22	1.67	1.685
	10		18.56		0.183		1.71	
	15		18.57		0.199		1.62	
	20		18.74		0.340		1.73	
EP/Zn-PVP-SPIO	5	47.48	14.99	14.99	0.441	0.46	1.47	1.483
	10		14.81		0.396		1.40	
	15		14.83		0.409		1.41	
	20		15.31		0.582		1.64	
EP/Mn-PVP-SPO	5	58.35	18.35	18.47	0.309	0.38	1.72	1.778
	10		18.50		0.390		1.80	
	15		18.46		0.386		1.77	
	20		18.56		0.452		1.82	
<i>KAS</i>								
EP as reference sample [31,32]	5	57.35	18.18	18.27	0.430	0.406	1.52	1.579
	10		17.96		0.163		1.42	
	15		18.39		0.464		1.66	
	20		18.54		0.569		1.71	
EP/PVP-SPIO	5	54.73	17.02	17.13	0.209	0.272	1.62	1.633
	10		17.08		0.238		1.66	
	15		17.12		0.253		1.57	
	20		17.31		0.389		1.68	
EP/Zn-PVP-SPIO	5	47.42	14.97	14.97	0.442	0.458	1.47	1.483
	10		14.79		0.397		1.40	
	15		14.81		0.409		1.41	
	20		15.29		0.583		1.64	
EP/Mn-PVP-SPO	5	54.59	17.12	17.28	0.355	0.424	1.68	1.736
	10		17.30		0.429		1.754	
	15		17.29		0.424		1.73	
	20		17.41		0.489		1.78	

3.2.2. Model Validation

Figure 5 compares the kinetics parameters derived from the experiments and those calculated theoretically. The rate of cure reaction ($d\alpha/dt$) was calculated by determining $f(\alpha)$. It can be confirmed that both calculated values (*Friedman* and *KAS*) are in good agreement with experimental data, except at the primary and last stages, which are insignificant.

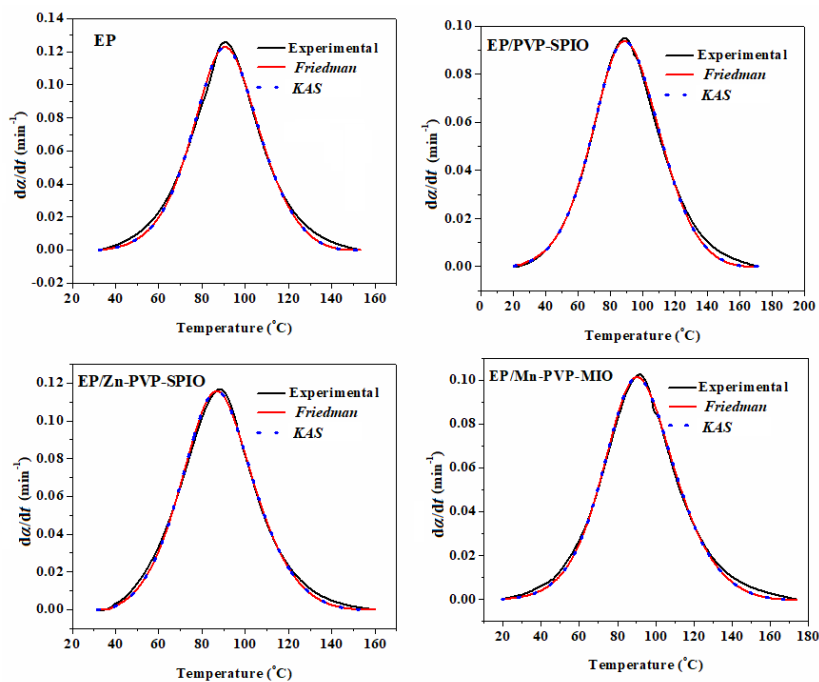


Figure 5. Comparison of experimental data on cure reaction rate with the outputs of the kinetic models for the samples crosslinked in DSC at a heating rate of 5 °C/min, based on the *Friedman* and *KAS* models.

4. Conclusions

In conclusion, the general mechanism explaining the curing reaction of epoxy and its nanocomposites remained unchanged by adding PVP-SPIO, Zn-PVP-SPIO, and Mn-PVP-SPIO nanofillers. Moreover, the presence of PVP-SPIO nanoparticles influenced the activation energy and led to lower amounts due to the hindrance effect of PVP-SPIO nanoparticles. However, the presentation of Zn dopant could subsequently improve the surface activity and the curing process of the system through a facilitated cure trend. Based on the *KAS* method, the average values of activation energy for neat epoxy and epoxy containing 0.1 wt.% Zn-PVP-SPIO and Mn-PVP-SPIO were found to be 57.35, 47.42, and 54.59 kJ/mol, respectively. The lower value of activation energy for the Zn-PVP-SPIO incorporated epoxy system compared to the epoxy containing Mn-PVP-SPIO can be attributed to its appropriate dispersion, which allowed for a higher surface area such that PVP groups available for reacting with epoxy played the key role.

Author Contributions: Conceptualization, M.R.S.; methodology, M.J.; software, M.J.; formal analysis, F.S.; investigation, M.J.; data curation, M.J.; writing—original draft preparation, M.J.; writing—review and editing, H.X.; supervision, M.R.S. and M.R.G.; All authors have read and agreed to the published version of the manuscript.

Funding: This research received no external funding.

Acknowledgments: Authors would like to thank the MDPI publisher for giving the authors the opportunity to publish this work.

Conflicts of Interest: The authors declare no conflict of interest.

Appendix A. Preparation and Characterization of Epoxy Nanocomposite

Appendix A.1. Chemicals

Epoxy matrix (Epon-828, epoxide equivalent weight of 185–192 g/eq) and curing agent (triethylenetetramine (TETA), hydrogen equivalent weight of 25 g/eq) were supplied by Hexion, Beijing, China.

Appendix A.2. Preparation of Epoxy Nanocomposites

First, 0.1 wt.% of bare PVP-SPIO, Zn-PVP-SPIO, and Mn-PVP-SPIO was added to epoxy resin to prepare the EP/PVP-SPIO, EP/Zn-PVP-SPIO, and EP/Mn-PVP-SPIO nanocomposites, respectively. After addition of nanoparticles, the mixture was sonicated for 5 min followed by mixing with a mechanical mixer at 2500 rpm for 20 min. Just before the DSC test, the stoichiometric amount of TETA was added to epoxy resin (13:100) and mixed slowly.

Appendix A.3. Characterization of Epoxy Nanocomposites

The cure reaction of the epoxy/amine system at the presence of 0.1 wt.% of bare PVP-SPIO, Zn-PVP-SPIO, and Mn-PVP-SPIO was investigated by DSC on Perkin Elmer DSC 4000. Dynamic DSC was performed at heating rates (β) of 5, 10, 15, and 20 °C/min from 15 to 250 °C by nitrogen flow rate of 20 mL/min.

Appendix B. Isoconversional Kinetic Methods

Friedman Model

The *Friedman* model is defined based on the following equation:

$$\ln \left[\beta_i \left(\frac{d\alpha}{dT} \right)_{\alpha,i} \right] = \ln [f(\alpha)A_\alpha] - \frac{E_\alpha}{RT_{\alpha,i}}, \quad (A1)$$

By plotting $\ln[\beta_i(d\alpha/dT)_{\alpha,i}]$ vs. $1/T_\alpha$, the value of activation energy (E_α) in each α can be obtained from the slope of Figure A1.

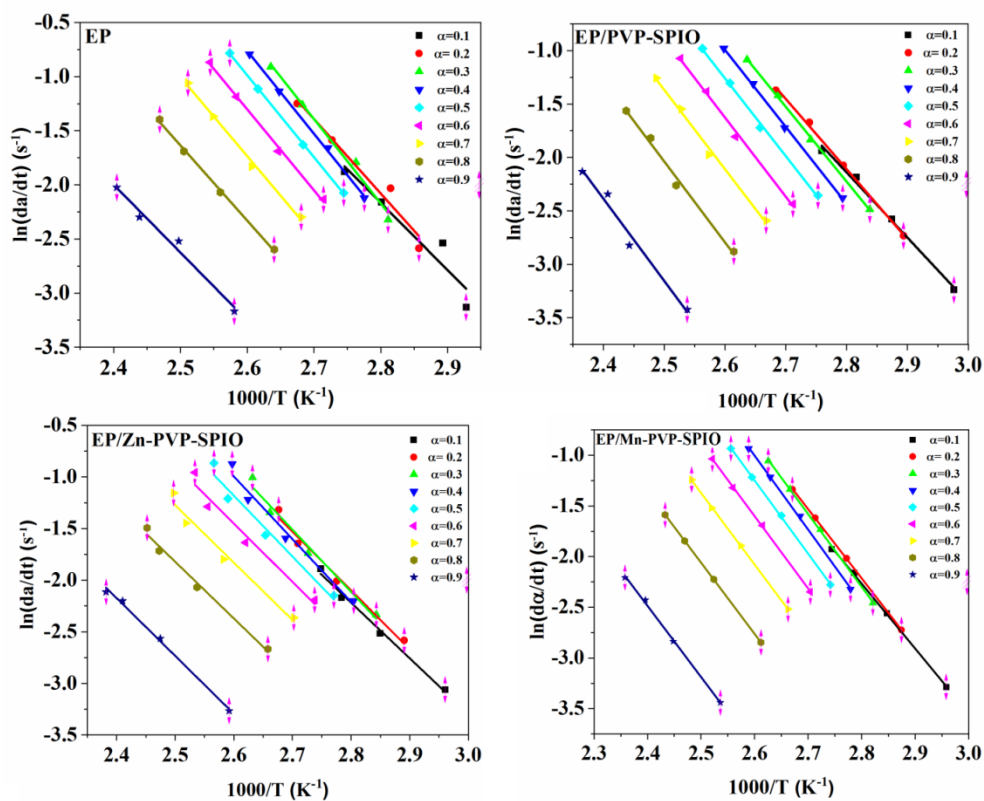


Figure A1. Plots of $\ln(d\alpha/dt)$ vs. $1/T$. The prepared samples based on *Friedman* model at $\beta = 5$ °C/min.

KAS Method

The KAS method was defined using the following equation:

$$\ln\left(\frac{\beta_i}{T_{\alpha,i}^{1.92}}\right) = Const - 1.0008\left(\frac{E_\alpha}{RT_\alpha}\right), \tag{A2}$$

Plotting $\ln(\beta_i/T_{\alpha,i}^{1.92})$ vs. $1/T_\alpha$ gives a straight line; its slope gives the activation energy (Figure A2).

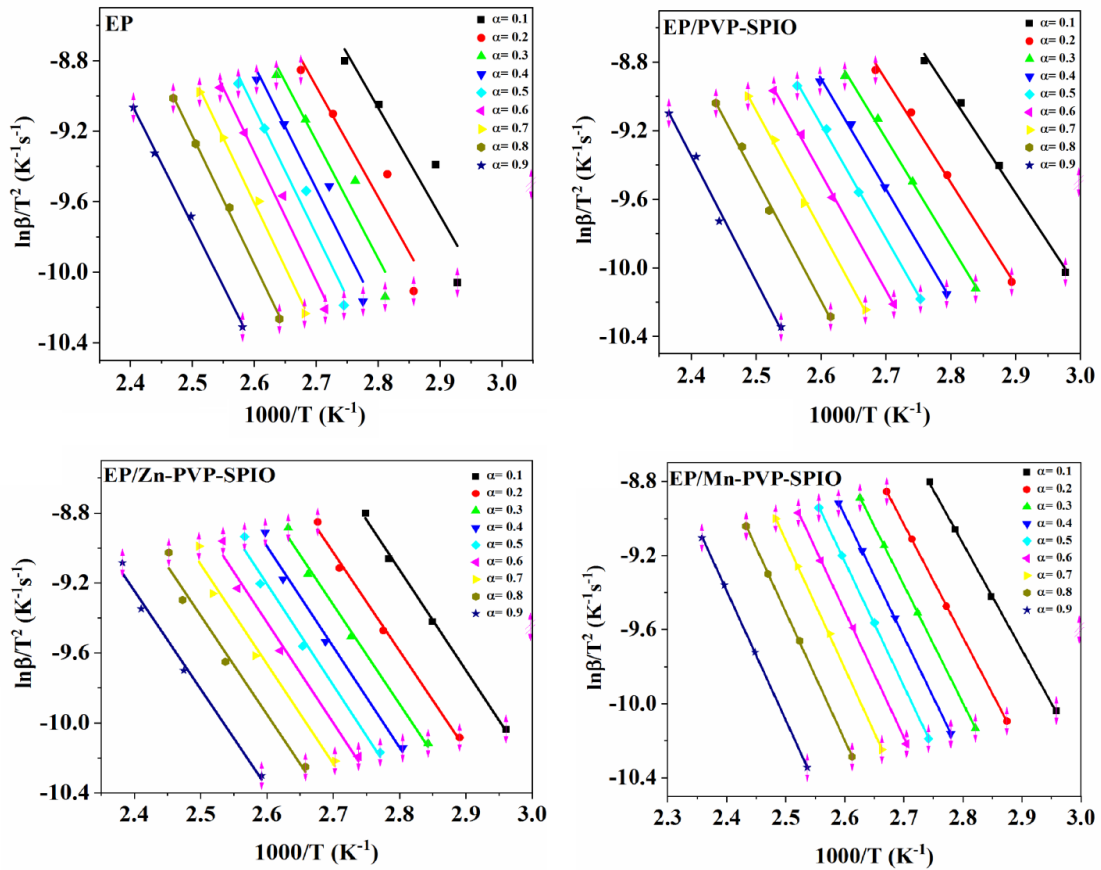


Figure A2. Plots of $\ln(\beta T^{1.92})$ vs. $1/T$ for prepared samples based on the KAS model.

Appendix C. Selection of Curing Reaction Model

Friedman Model

Based on the *Friedman* method, the model of epoxy curing reaction can be determined using Equation (A3). The shape of plot of $\ln[Af(\alpha)]$ vs. $\ln(1 - \alpha)$ denotes the deviation from nth-order reaction (Figure A3).

$$\ln[Af(\alpha)] = \ln\left(\frac{d\alpha}{dt}\right) + \frac{E}{RT} = \ln A + n \ln(1 - \alpha), \tag{A3}$$

For the nth-order cure mechanism, a straight line was obtained by plotting $\ln[Af(\alpha)]$ vs. $\ln(1 - \alpha)$, whose slope gives the reaction degree (n).

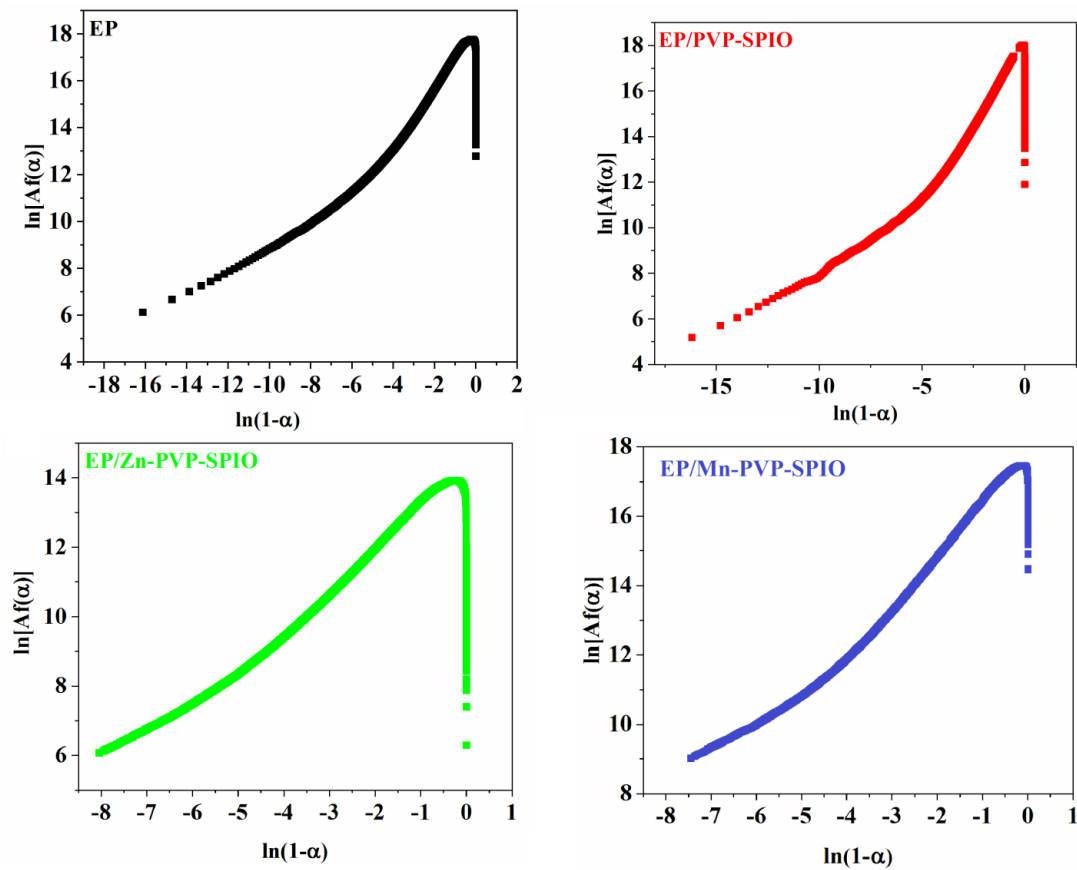


Figure A3. Plots of $\ln[Af(\alpha)]$ vs. $\ln(1 - \alpha)$ for the samples under a heating rate of $5\text{ }^\circ\text{C}/\text{min}$ used in calculation of activation energy via the *Friedman* method.

Malek Method

The kinetic model based on the *Malek* method is determined using the following equations:

$$y(\alpha) = \left(\frac{d\alpha}{dt}\right)_\alpha \exp\left(\frac{E_0}{RT_\alpha}\right) = Af(\alpha), \tag{A4}$$

$$z(\alpha) = \left(\frac{d\alpha}{dt}\right)_\alpha T_\alpha^2 \left[\frac{\pi(x)}{\beta T_\alpha}\right], \tag{A5}$$

The term in the brackets of Equation (A5) has no significant effect on the shape of the $z(\alpha)$ function and can be omitted. In Equation (A4), the amount of E_0 is determined via the *Flynn–Wall–Ozawa (FWO)* method, where the change in the activation energy with variation of α remains constant, from the following equation:

$$\ln(\beta_i) = Const - 1.052 \left(\frac{E_\alpha}{RT_\alpha}\right), \tag{A6}$$

In the *FWO* method, activation energy is determined from the slope of $\ln(\beta_i)$ vs. $1/T$, as shown in Figure A4.

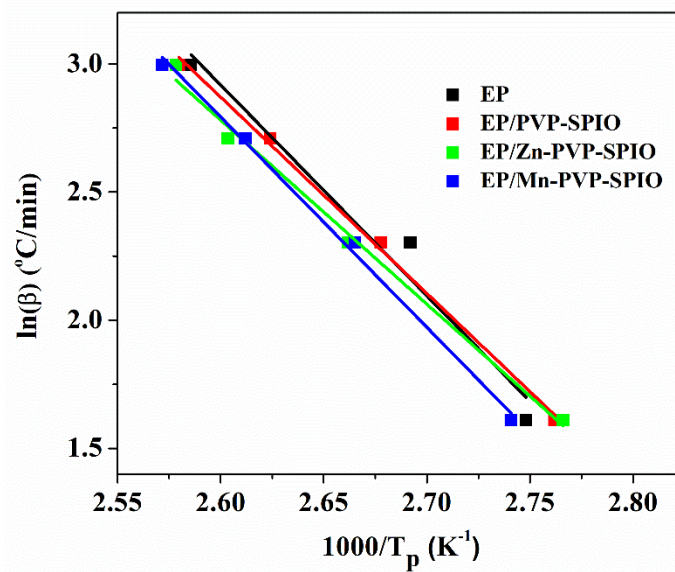


Figure A4. Plots of $\ln(\beta)$ vs. $1/T$ for epoxy resin and prepared nanocomposites derived from the Flynn–Wall–Ozawa (FWO) model.

This method gives the activation energy independent of conversion. Via the FWO method, the values of activation energy are found to be 64.9, 55.3, 52.6, and 64.86 kJ/mol for neat epoxy, EP/PVP-SPIO, EP/PVP-SPIO, and EP/Mn-PVP-SPIO, respectively.

The experimental values of $y(\alpha)$ and $z(\alpha)$ for the EP, EP/PVP-SPIO, EP/Zn-PVP-SPIO, and EP/Zn-PVP-SPIO nanocomposites as a function of conversion are shown in Figure A5 and compared with theoretical master plots.

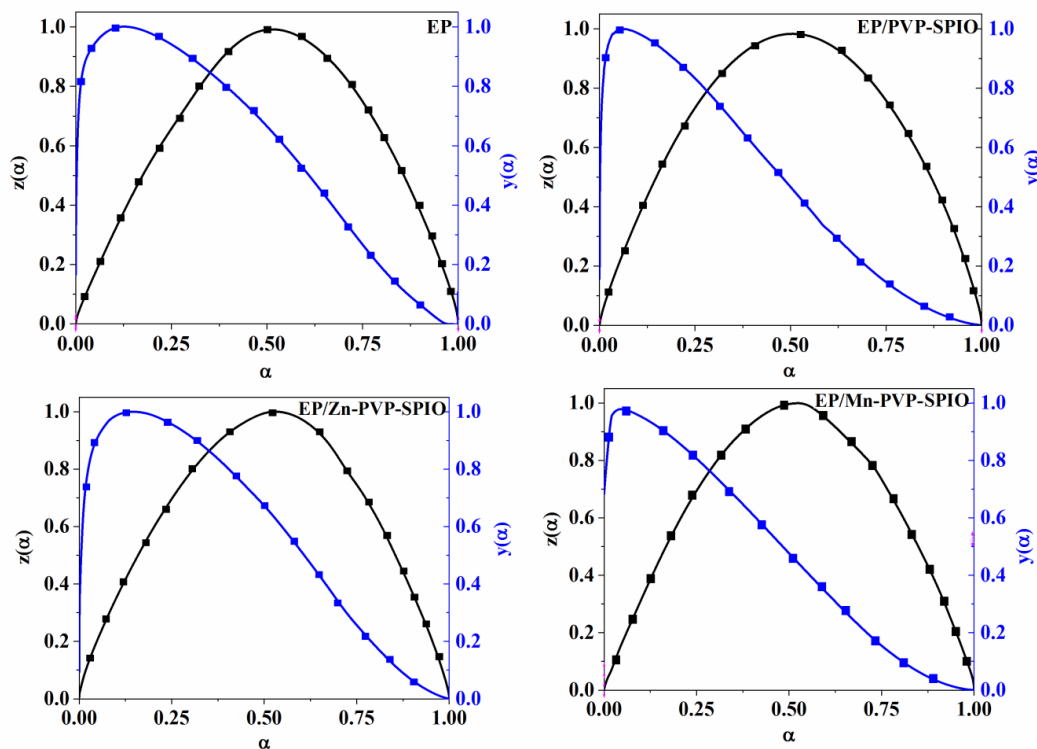


Figure A5. Variation of $y(\alpha)$ and $z(\alpha)$ versus conversion for prepared samples based on the Malek model.

$y(\alpha)$ and $z(\alpha)$ was normalized as follows to vary between 0 and 1:

$$y_n(\alpha) = \frac{y(\alpha)}{\max [y(\alpha)]}, \tag{A7}$$

$$z_n(\alpha) = \frac{z(\alpha)}{\max [z(\alpha)]}, \tag{A8}$$

The maximum values, $\max[y(\alpha)] = \alpha_m$ and $\max[z(\alpha)] = \alpha_p$, can be found from the following expressions:

$$f'(\alpha_m) = 0, \tag{A9}$$

$$f'(\alpha_p) g(\alpha_p) = -1, \tag{A10}$$

Appendix D. Determination of Degree of Reaction

The degrees of autocatalytic reaction (n and m) and the pre-exponential factor (A) can be determined through the following equations:

$$ValueI = \ln\left(\frac{d\alpha}{dt}\right) + \frac{E_\alpha}{RT} - \ln\left[\frac{d(1-\alpha)}{dt}\right] - \frac{E_\alpha}{RT'} = (n-m)\ln\left(\frac{1-\alpha}{\alpha}\right), \tag{A11}$$

$$ValueII = \ln\left(\frac{d\alpha}{dt}\right) + \frac{E_\alpha}{RT} + \ln\left[\frac{d(1-\alpha)}{dt}\right] + \frac{E_\alpha}{RT'} = (n+m)\ln(\alpha - \alpha^2) + 2\ln A, \tag{A12}$$

The slope of the plot of $ValueI$ vs. $\ln[(1-\alpha)/\alpha]$ (Figure A6) gives the value of $(n-m)$, and the slope and intercept of the plot of $ValueII$ vs. $\ln(\alpha - \alpha^2)$ (Figure A7) give the value of $(n+m)$ and $2\ln A$.

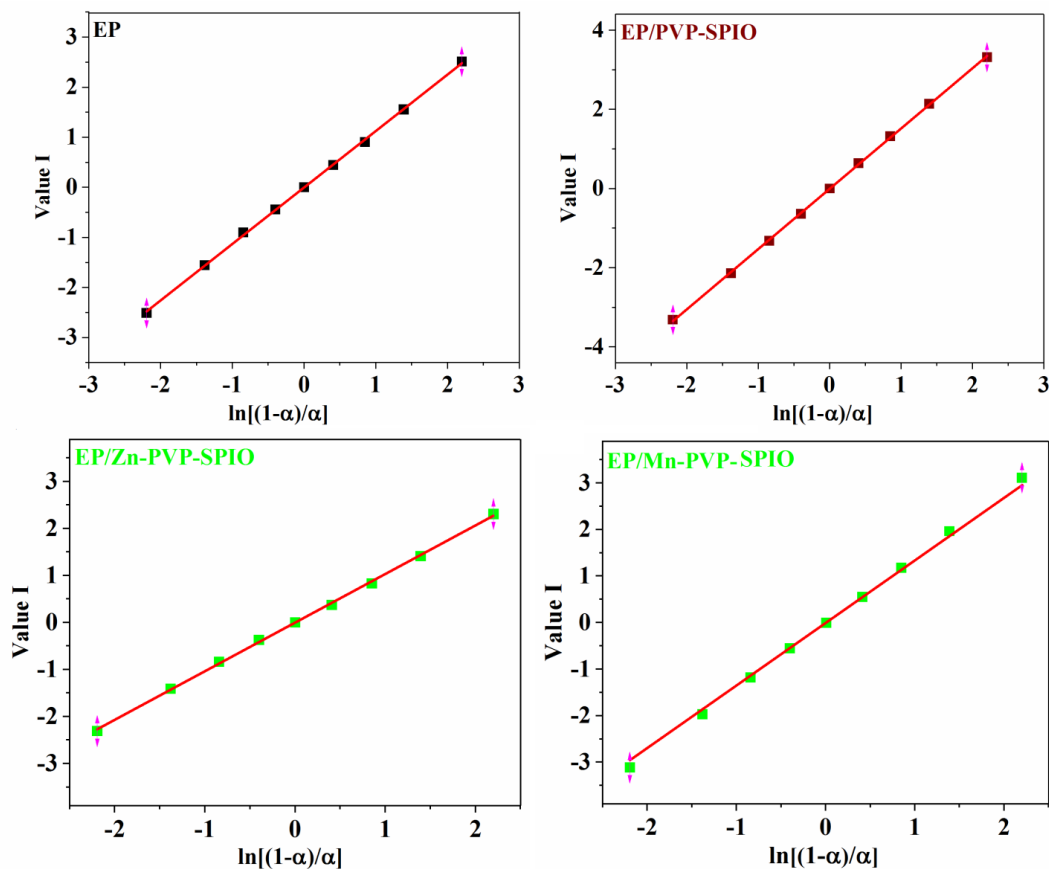


Figure A6. Plots of $Value I$ calculated using DSC data for the prepared epoxy system under a heating rate of $5\text{ }^\circ\text{C}/\text{min}$.

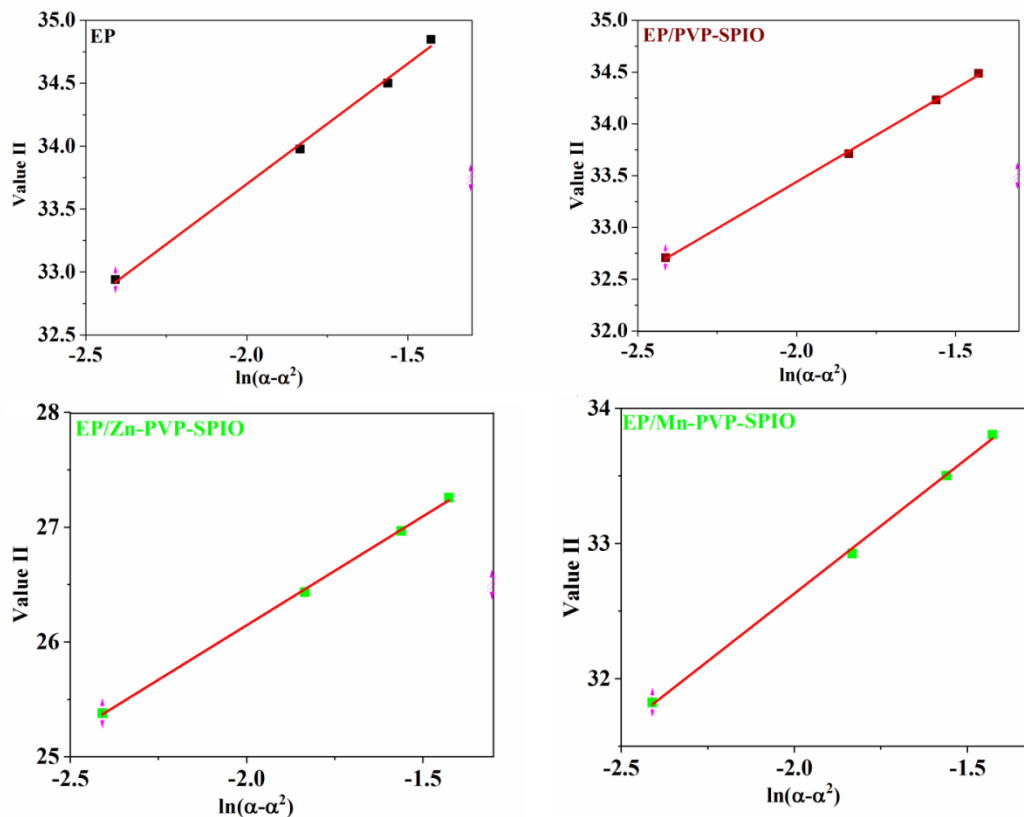


Figure A7. Plots of Value II calculated for the prepared samples under a heating rate of 5 °C/min.

References

- Jouyandeh, M.; Jazani, O.M.; Navarchian, A.H.; Shabani, M.; Vahabi, H.; Saeb, M.R. Surface engineering of nanoparticles with macromolecules for epoxy curing: Development of super-reactive nitrogen-rich nanosilica through surface chemistry manipulation. *Appl. Surf. Sci.* **2018**, *447*, 152–164. [CrossRef]
- Puglia, D.; Valentini, L.; Armentano, I.; Kenny, J. Effects of single-walled carbon nanotube incorporation on the cure reaction of epoxy resin and its detection by Raman spectroscopy. *Diam. Relat. Mater.* **2003**, *12*, 827–832. [CrossRef]
- Mauro, M.; Acocella, M.R.; Corcione, C.E.; Maffezzoli, A.; Guerra, G. Catalytic activity of graphite-based nanofillers on cure reaction of epoxy resins. *Polymer* **2014**, *55*, 5612–5615. [CrossRef]
- Aliakbari, M.; Jazani, O.M.; Sohrabian, M.; Jouyandeh, M.; Saeb, M.R. Multi-nationality epoxy adhesives on trial for future nanocomposite developments. *Prog. Org. Coat.* **2019**, *133*, 376–386. [CrossRef]
- Jouyandeh, M.; Moini Jazani, O.; Navarchian, A.H.; Saeb, M.R. High-performance epoxy-based adhesives reinforced with alumina and silica for carbon fiber composite/steel bonded joints. *J. Reinf. Plast. Compos.* **2016**, *35*, 1685–1695. [CrossRef]
- Wan, J.; Gan, B.; Li, C.; Molina-Aldareguia, J.; Kalali, E.N.; Wang, X.; Wang, D.-Y. A sustainable, eugenol-derived epoxy resin with high biobased content, modulus, hardness and low flammability: Synthesis, curing kinetics and structure–property relationship. *Chem. Eng. J.* **2016**, *284*, 1080–1093. [CrossRef]
- Jouyandeh, M.; Paran, S.M.R.; Jannesari, A.; Saeb, M.R. ‘Cure Index’ for thermoset composites. *Prog. Org. Coat.* **2019**, *127*, 429–434. [CrossRef]
- Tikhani, F.; Jouyandeh, M.; Jafari, S.H.; Chabokrow, S.; Ghahari, M.; Gharanjig, K.; Klein, F.; Hampp, N.; Ganjali, M.R.; Formela, K.; et al. Cure Index demonstrates curing of epoxy composites containing silica nanoparticles of variable morphology and porosity. *Prog. Org. Coat.* **2019**, *135*, 176–184. [CrossRef]
- Akbari, V.; Najafi, F.; Vahabi, H.; Jouyandeh, M.; Badawi, M.; Morisset, S.; Ganjali, M.R.; Saeb, M.R. Surface chemistry of halloysite nanotubes controls the curability of low filled epoxy nanocomposites. *Prog. Org. Coat.* **2019**, *135*, 555–564. [CrossRef]

10. Vyazovkin, S.; Burnham, A.K.; Criado, J.M.; Pérez-Maqueda, L.A.; Popescu, C.; Sbirrazzuoli, N. ICTAC Kinetics Committee recommendations for performing kinetic computations on thermal analysis data. *Thermochim. Acta* **2011**, *520*, 1–19. [[CrossRef](#)]
11. Lu, L.; Xia, L.; Zengheng, H.; Xingyue, S.; Yi, Z.; Pan, L. Investigation on cure kinetics of epoxy resin containing carbon nanotubes modified with hyper-branched polyester. *RSC Adv.* **2018**, *8*, 29830–29839. [[CrossRef](#)]
12. Karami, Z.; Jouyandeh, M.; Hamad, S.M.; Ganjali, M.R.; Aghazadeh, M.; Torre, L.; Puglia, D.; Saeb, M.R. Curing epoxy with Mg-Al LDH nanoplatelets intercalated with carbonate ion. *Prog. Org. Coat.* **2019**, *136*, 105278. [[CrossRef](#)]
13. Karami, Z.; Jouyandeh, M.; Ghiyasi, S.; Ali, J.A.; Ganjali, M.R.; Aghazadeh, M.; Maadani, M.; Rallini, M.; Luzi, F.; Torre, L.; et al. Exploring curing potential of epoxy nanocomposites containing nitrate anion intercalated Mg-Al-LDH with Cure Index. *Prog. Org. Coat.* **2020**, *139*, 105255. [[CrossRef](#)]
14. Karami, Z.; Jouyandeh, M.; Ali, J.A.; Ganjali, M.R.; Aghazadeh, M.; Paran, S.M.R.; Naderi, G.; Puglia, D.; Saeb, M.R. Epoxy/layered double hydroxide (LDH) nanocomposites: Synthesis, characterization, and Excellent cure feature of nitrate anion intercalated Zn-Al LDH. *Prog. Org. Coat.* **2019**, *136*, 105218. [[CrossRef](#)]
15. Karami, Z.; Aghazadeh, M.; Jouyandeh, M.; Zarrintaj, P.; Vahabi, H.; Ganjali, M.R.; Torre, L.; Puglia, D.; Saeb, M.R. Epoxy/Zn-Al-CO₃ LDH nanocomposites: Curability assessment. *Prog. Org. Coat.* **2020**, *138*, 105355. [[CrossRef](#)]
16. Karami, Z.; Jouyandeh, M.; Ali, J.A.; Ganjali, M.R.; Aghazadeh, M.; Maadani, M.; Rallini, M.; Luzi, F.; Torre, L.; Puglia, D.; et al. Development of Mg-Zn-Al-CO₃ ternary LDH and its curability in epoxy/amine system. *Prog. Org. Coat.* **2019**, *136*, 105264. [[CrossRef](#)]
17. Karami, Z.; Jouyandeh, M.; Ali, J.A.; Ganjali, M.R.; Aghazadeh, M.; Maadani, M.; Rallini, M.; Luzi, F.; Torre, L.; Puglia, D.; et al. Cure Index for labeling curing potential of epoxy/LDH nanocomposites: A case study on nitrate anion intercalated Ni-Al-LDH. *Prog. Org. Coat.* **2019**, *136*, 105228. [[CrossRef](#)]
18. Jouyandeh, M.; Ganjali, M.R.; Ali, J.A.; Aghazadeh, M.; Stadler, F.J.; Saeb, M.R. Curing epoxy with electrochemically synthesized Mn_xFe_{3-x}O₄ magnetic nanoparticles. *Prog. Org. Coat.* **2019**, *136*, 105199. [[CrossRef](#)]
19. Jouyandeh, M.; Ganjali, M.R.; Ali, J.A.; Aghazadeh, M.; Stadler, F.J.; Saeb, M.R. Curing epoxy with electrochemically synthesized Ni_xFe_{3-x}O₄ magnetic nanoparticles. *Prog. Org. Coat.* **2019**, *136*, 105198. [[CrossRef](#)]
20. Jouyandeh, M.; Ganjali, M.R.; Ali, J.A.; Aghazadeh, M.; Stadler, F.J.; Saeb, M.R. Curing epoxy with electrochemically synthesized Co_xFe_{3-x}O₄ magnetic nanoparticles. *Prog. Org. Coat.* **2019**, *137*, 105252. [[CrossRef](#)]
21. Jouyandeh, M.; Zarrintaj, P.; Ganjali, M.R.; Ali, J.A.; Karimzadeh, I.; Aghazadeh, M.; Ghaffari, M.; Saeb, M.R. Curing epoxy with electrochemically synthesized Gd_xFe_{3-x}O₄ magnetic nanoparticles. *Prog. Org. Coat.* **2019**, *136*, 105245. [[CrossRef](#)]
22. Jouyandeh, M.; Ali, J.A.; Aghazadeh, M.; Formela, K.; Saeb, M.R.; Ranjbar, Z.; Ganjali, M.R. Curing epoxy with electrochemically synthesized Zn_xFe_{3-x}O₄ magnetic nanoparticles. *Prog. Org. Coat.* **2019**, *136*, 105246. [[CrossRef](#)]
23. Jouyandeh, M.; Ganjali, M.R.; Hadavand, B.S.; Aghazadeh, M.; Akbari, V.; Shammiry, F.; Saeb, M.R. Curing epoxy with polyvinyl chloride (PVC) surface-functionalized Co_xFe_{3-x}O₄ nanoparticles. *Prog. Org. Coat.* **2019**, *137*, 105364. [[CrossRef](#)]
24. Jouyandeh, M.; Ganjali, M.R.; Ali, J.A.; Akbari, V.; Karami, Z.; Aghazadeh, M.; Zarrintaj, P.; Saeb, M.R. Curing epoxy with polyethylene glycol (PEG) surface-functionalized Gd_xFe_{3-x}O₄ magnetic nanoparticles. *Prog. Org. Coat.* **2019**, *137*, 105283. [[CrossRef](#)]
25. Jouyandeh, M.; Hamad, S.M.; Karimzadeh, I.; Aghazadeh, M.; Karami, Z.; Akbari, V.; Shammiry, F.; Formela, K.; Saeb, M.R.; Ranjbar, Z.; et al. Unconditionally blue: Curing epoxy with polyethylene glycol (PEG) surface-functionalized Zn_xFe_{3-x}O₄ magnetic nanoparticles. *Prog. Org. Coat.* **2019**, *137*, 105285. [[CrossRef](#)]
26. Jouyandeh, M.; Karami, Z.; Ali, J.A.; Karimzadeh, I.; Aghazadeh, M.; Laoutid, F.; Vahabi, H.; Saeb, M.R.; Ganjali, M.R.; Dubois, P. Curing epoxy with polyethylene glycol (PEG) surface-functionalized Ni_xFe_{3-x}O₄ magnetic nanoparticles. *Prog. Org. Coat.* **2019**, *136*, 105250. [[CrossRef](#)]

27. Jouyandeh, M.; Ganjali, M.R.; Ali, J.A.; Aghazadeh, M.; Karimzadeh, I.; Formela, K.; Colom, X.; Cañavate, J.; Saeb, M.R. Curing epoxy with ethylenediaminetetraacetic acid (EDTA) surface-functionalized $\text{CoFe}_3\text{-xO}_4$ magnetic nanoparticles. *Prog. Org. Coat.* **2019**, *136*, 105248. [[CrossRef](#)]
28. Jouyandeh, M.; Ali, J.A.; Akbari, V.; Aghazadeh, M.; Paran, S.M.R.; Naderi, G.; Saeb, M.R.; Ranjbar, Z.; Ganjali, M.R. Curing epoxy with polyvinylpyrrolidone (PVP) surface-functionalized $\text{MnFe}_3\text{-xO}_4$ magnetic nanoparticles. *Prog. Org. Coat.* **2019**, *136*, 105247. [[CrossRef](#)]
29. Jouyandeh, M.; Ganjali, M.R.; Ali, J.A.; Aghazadeh, M.; Saeb, M.R.; Ray, S.S. Curing epoxy with polyvinylpyrrolidone (PVP) surface-functionalized $\text{NiFe}_3\text{-xO}_4$ magnetic nanoparticles. *Prog. Org. Coat.* **2019**, *136*, 105259. [[CrossRef](#)]
30. Jouyandeh, M.; Ganjali, M.R.; Ali, J.A.; Aghazadeh, M.; Paran, S.M.R.; Naderi, G.; Saeb, M.R.; Thomas, S. Curing epoxy with polyvinylpyrrolidone (PVP) surface-functionalized $\text{ZnFe}_3\text{-xO}_4$ magnetic nanoparticles. *Prog. Org. Coat.* **2019**, *136*, 105227. [[CrossRef](#)]
31. Jouyandeh, M.; Karami, Z.; Hamad, S.M.; Ganjali, M.R.; Akbari, V.; Vahabi, H.; Kim, S.-J.; Zarrintaj, P.; Saeb, M.R. Nonisothermal cure kinetics of epoxy/ $\text{ZnFe}_3\text{-xO}_4$ nanocomposites. *Prog. Org. Coat.* **2019**, *136*, 105290. [[CrossRef](#)]
32. Jouyandeh, M.; Paran, S.M.R.; Khadem, S.S.M.; Ganjali, M.R.; Akbari, V.; Vahabi, H.; Saeb, M.R. Nonisothermal cure kinetics of epoxy/ $\text{MnFe}_3\text{-xO}_4$ nanocomposites. *Prog. Org. Coat.* **2020**, *140*, 105505. [[CrossRef](#)]
33. Jouyandeh, M.; Paran, S.M.R.; Jannesari, A.; Puglia, D.; Saeb, M.R. Protocol for nonisothermal cure analysis of thermoset composites. *Prog. Org. Coat.* **2019**, *131*, 333–339. [[CrossRef](#)]
34. Jouyandeh, M.; Tikhani, F.; Shabaniyan, M.; Movahedi, F.; Moghari, S.; Akbari, V.; Gabrion, X.; Laheurte, P.; Vahabi, H.; Saeb, M.R. Synthesis, characterization, and high potential of 3D metal–organic framework (MOF) nanoparticles for curing with epoxy. *J. Alloy. Compd.* **2020**, *829*, 154547. [[CrossRef](#)]
35. Jouyandeh, M.; Karami, Z.; Moini Jazani, O.; Formela, K.; Paran, S.M.R.; Jannesari, A.; Saeb, M.R. Curing epoxy resin with anhydride in the presence of halloysite nanotubes: The contradictory effects of filler concentration. *Prog. Org. Coat.* **2019**, *126*, 129–135. [[CrossRef](#)]
36. Saeb, M.R.; Rastin, H.; Nonahal, M.; Ghaffari, M.; Jannesari, A.; Formela, K. Cure kinetics of epoxy/MWCNTs nanocomposites: Nonisothermal calorimetric and rheokinetic techniques. *J. Appl. Polym. Sci.* **2017**, *134*, 45221. [[CrossRef](#)]
37. Dimier, F.; Sbirrazzuoli, N.; Vergnes, B.; Vincent, M. Curing kinetics and chemorheological analysis of polyurethane formation. *Polym. Eng. Sci.* **2004**, *44*, 518–527. [[CrossRef](#)]
38. Wan, J.; Li, C.; Bu, Z.-Y.; Xu, C.-J.; Li, B.-G.; Fan, H. A comparative study of epoxy resin cured with a linear diamine and a branched polyamine. *Chem. Eng. J.* **2012**, *188*, 160–172. [[CrossRef](#)]
39. Paran, S.M.R.; Vahabi, H.; Jouyandeh, M.; Ducos, F.; Formela, K.; Saeb, M.R. Thermal decomposition kinetics of dynamically vulcanized polyamide 6–acrylonitrile butadiene rubber–halloysite nanotube nanocomposites. *J. Appl. Polym. Sci.* **2019**, *136*, 47483. [[CrossRef](#)]
40. Vyazovkin, S. Model-free kinetics. *J. Therm. Anal. Calorim.* **2006**, *83*, 45–51. [[CrossRef](#)]
41. Ratna, D. *Handbook of Thermoset Resins*; Ismithers: Shawbury, UK, 2009.
42. Akbari, V.; Jouyandeh, M.; Paran, S.M.R.; Ganjali, M.R.; Abdollahi, H.; Vahabi, H.; Ahmadi, Z.; Formela, K.; Esmaili, A.; Mohaddespour, A. Effect of Surface Treatment of Halloysite Nanotubes (HNTs) on the Kinetics of Epoxy Resin Cure with Amines. *Polymers* **2020**, *12*, 930. [[CrossRef](#)] [[PubMed](#)]
43. Tikhani, F.; Moghari, S.; Jouyandeh, M.; Laoutid, F.; Vahabi, H.; Saeb, M.R.; Dubois, P. Curing Kinetics and Thermal Stability of Epoxy Composites Containing Newly Obtained Nano-Scale Aluminum Hypophosphite (AlPO_2). *Polymers* **2020**, *12*, 644. [[CrossRef](#)] [[PubMed](#)]
44. Jouyandeh, M.; Yarahmadi, E.; Didehban, K.; Ghiyasi, S.; Paran, S.M.R.; Puglia, D.; Ali, J.A.; Jannesari, A.; Saeb, M.R.; Ranjbar, Z.; et al. Cure kinetics of epoxy/graphene oxide (GO) nanocomposites: Effect of starch functionalization of GO nanosheets. *Prog. Org. Coat.* **2019**, *136*, 105217. [[CrossRef](#)]

